



**HAL**  
open science

## Investigation of the mechanical and thermal performances of concrete hollow blocks

Emilio Sassine, Yassine Cherif, Joseph Dgheim, Emmanuel Antczak

► **To cite this version:**

Emilio Sassine, Yassine Cherif, Joseph Dgheim, Emmanuel Antczak. Investigation of the mechanical and thermal performances of concrete hollow blocks. SN Applied Sciences, 2020, 10.1007/S42452-020-03881-X . hal-03209135

**HAL Id: hal-03209135**

**<https://hal.science/hal-03209135>**

Submitted on 23 Mar 2022

**HAL** is a multi-disciplinary open access archive for the deposit and dissemination of scientific research documents, whether they are published or not. The documents may come from teaching and research institutions in France or abroad, or from public or private research centers.

L'archive ouverte pluridisciplinaire **HAL**, est destinée au dépôt et à la diffusion de documents scientifiques de niveau recherche, publiés ou non, émanant des établissements d'enseignement et de recherche français ou étrangers, des laboratoires publics ou privés.

# Investigation of the mechanical and thermal performances of concrete hollow blocks

Emilio SASSINE<sup>1,\*</sup>; Yassine CHERIF<sup>2</sup>; Joseph DGHEIM<sup>1</sup>; Emmanuel ANTCZAK<sup>2</sup>

<sup>1</sup>Laboratory of Applied Physics (LPA), Group of Mechanical Thermal and Renewable Energies (GMTER), Lebanese University, Faculty of Sciences, Fanar Campus, Lebanon

<sup>2</sup>Artois University, ULR 4515, Laboratoire de Génie Civil et géo-Environnement (LGCgE), Béthune, F-62400, France.

## Abstract

In order to improve the thermal performance of external masonry walls, the impact of the blocks' internal configuration on both their mechanical strength and thermal properties is numerically investigated. Ten different configurations with approximatively similar void ratios of about 40% (38.25% - 40.5%) and same external dimensions (40 cm x 20 cm x 10 cm) were compared thermally and mechanically in order to investigate the effect of bulkheads on their performance and to promote some design guidelines. The complexity of the heat transfer phenomena inside the blocks as well as the stress distribution for vertical and lateral loads are detailed, leading to a better understanding of their thermal and mechanical behaviors. The numerical results indicated that the longitudinal bulkheads improve the thermal resistance of the blocks and thus reduce the heat flux passing through the blocks, while the transversal bulkheads reduce the thermal performance of the hollow blocks by creating heat bridges inside their structure. On the other hand, the mechanical behavior of the investigated blocks varies very slightly between the investigated models in vertical compression in the  $z$ -axis direction which reduces the influence of this parameter in the selection of the best shape configuration. However, the mechanical resistance to side compression increases by increasing the transversal bulkheads and decreasing the number of longitudinal bulkheads.

## Keywords

Hollow block design, heat modeling, mechanical modeling, thermal resistance, principal stresses

*\*Corresponding author:*

Emilio SASSINE, Email address: [emilio.sassine@gmail.com](mailto:emilio.sassine@gmail.com), Laboratoire de Physique Appliquée (LPA), Université Libanaise, Faculté des Sciences, Campus Fanar, Lebanon.

Yassine CHERIF, Email address: [yassine.cherif@univ-artois.fr](mailto:yassine.cherif@univ-artois.fr), Univ. Artois, ULR 4515, Laboratoire de Génie Civil et géo-Environnement (LGCgE), Béthune, F-62400, France.

## 1 Introduction

Masonry hollow blocks are widely used as construction materials for what they offer as advantages in terms of physical properties (mechanical resistance, thermal and sound insulation, fire resistance, life span), low cost, low maintenance, and ease of implementation. The ever growing international interest related to the energy efficiency in buildings has led to many scientific and industrial efforts towards the improvement of masonry units in order to meet nowadays' energy saving requirements. These improvements can be made either by modifying the concrete mixture for reducing its thermal conductivity and thus reducing the conductive heat flow across the blocks, by filling the air cavities by insulation material, or by modifying the block configuration (vertical and horizontal bulkheads and cavities shape). However, this modification alters the mechanical properties of the block, especially its resistance to compression. The purpose of this work is to explore the effect of the block configuration on its thermal and mechanical properties so as to better understand the relationship between these parameters and the selection criteria of a given configuration.

Many studies discussed the thermal improvement potential of building blocks by either modifying the concrete composition [1-3], or hollow block's configuration. Urban et al. [4] compared different hollow blocks geometries available in the market by using numerical simulation methods. Fogiatto et al. [5] examined the best thermal resistance for ten different blocks by varying the cavity configuration using the same external dimensions using ANSYS®. Kanellopoulos et al. [6] performed a transient thermal analysis using the finite element method (FEM) to determine the thermal response of a perforated clay brick masonry wall. Coz Diaz et al. [7] optimized lightweight hollow blocks used in internal floors by varying the number of vertical and horizontal intermediate bulkheads preserving constant external dimensions. He found that the horizontal intermediate bulkheads and the thermal conductivity of the concrete mixture were the main parameters influencing the thermal performance. Zhang et al. [8] also ranked the principal factors influencing the dynamic thermal performance in descending order as follows: the thermal conductivity, the thermal capacity, the thermal conductivity of the inserted material inside the cavities, the block thickness, and the number of hole rows. Martinez et al. [9] evaluated the effect of the thermal conductivity of the solid mixture, the geometry, and adding insulation materials on the heat flux, the distribution of temperatures, and the air velocity field inside the cavities, through experimental measurements and numerical simulations using ANSYS Fluent®.

In addition to the thermal studies related to concrete hollow blocks, their mechanical behavior was also examined at the block scale level in many research works. Barbosa et al. [10] analyzed numerically the behavior of hollow concrete blocks under uniaxial compression. Their numerical results were compared to the masonry unit experimental ones. The elastic and inelastic parameters (compressive strength, tensile strength, stress-strain relationships and fracture energy) were acquired from concrete samples that constitute the blocks. Ben Ayed et al. [11] carried out compressive tests on superposed Interlocking Stabilized Earth Block (ISEB) that are laid dry without grout mortar. These tests showed that the contact area and the clearance between the blocks decreased the masonry's compressive strength. A simplified spring model was considered for estimating the apparent Young's modulus of the wall. Arun et al. [12] explored the compressive and flexural characteristics of concrete composite and expanded polystyrene (EPS) block under standard loading condition as well as their thermal performance using *R*-value. The proposed system helps in sustainable building construction by affording high thermal insulation with improved structural strength. Javadi et al. [13] used recycled concrete aggregates from demolition wastes and compared their durability and mechanical strength to bio-blocks produced with natural aggregates.

The impact of the block design on its mechanical properties was studied by Coz Diaz et al. [14] who used the finite element method and a combined Drucker–Prager and Willam–Warnke material models for concrete to compute the compressive resistance of different concrete blocks and determine the optimum hollow block from the handling and structural points of view. Javidan et al. [15] performed a numerical research for an optimum shape of hollow blocks based on the ratio the compressive strength and the weight.

The interrelation between thermal and mechanical performance study of masonry blocks based on their mixture composition has been the subject of various works. Caruana et al. [16] optimized a hollow block mix design searching for improving its thermal properties without compromising its physical (compressive strength) and geometrical properties (external dimensions). Mohammed et al. [17] evaluated miscellaneous physical properties (thermal conductivity, compressive strength, acoustic absorption and other...) concrete blocks mixed with a crumb rubber concrete mixture. Su et al. [18] determined the mechanical strength and thermal properties of an optimized hollow block consisting of an extruded polystyrene layer fixed between an internal hollow concrete block part and an external concrete decoration layer. Experimental measurements and numerical simulations were performed for this purpose. Sutcu et al. [19] studied the mechanical strength and the thermal properties for hollow clay bricks made up with different paper waste concentrations. Xu et al. [20] studied experimentally the effect of wood fibers content on the thermal and mechanical properties of autoclaved aerated concrete.

In this work, the mechanical and thermal behaviors of concrete hollow blocks are simultaneously studied by varying the blocks' internal shape aiming at determining the optimal hollow block design providing the optimal compromise between thermal resistance and mechanical resistance by examining ten different hollow block configurations. The heat flow inside the blocks is visualized numerically and the main parameters affecting the thermal performance are discussed. Heat conduction through the solid concrete matrix as well as convective and radiative heat flows inside the air cavities were visualized and discussed to highlight the effect of the block geometrical parameters on its thermal performance. The mechanical behavior of the block was investigated in two different load configurations: the first one consisting of a vertical compression in the  $z$ -axis direction and a lateral compression in the  $y$ -axis direction.

## 2 Scope of the study

Ten different configurations were considered with approximately similar void ratios of about 40% (38.25% - 40.5%). All the blocks have the same external dimensions (40 cm x 20 cm x 10 cm), they present hollows and are closed from the bottom with a 2 cm concrete thickness. They differ by the number and the shape of the cavities. The dimensions of the studied blocks are reported in Table 1.

**Table 1- Configurations and dimension of the 10 tested cases**

Block Model	Block configuration	Block name	Cavities dimensions (cm x cm)
#1		1 cavity	34 x 5
#2		2 cavities, 1 row	17 x 5.2
#3		2 cavities, 2 rows	36 x 2.5
#4		3 cavities, 1 row	10 x 6
#5		4 cavities, 1 row	7.5 x 6
#6		4 cavities 2 x 2	17 x 2.6
#7		6 cavities 3 x 2	11 x 2.7
#8		8 cavities 4 x 2	8 x 2.8
#9		8 cavities + alternation	3.2 x 2.8 / 8 x 2.8
#10		Lebanese hollow block	R 2.8 / a 8.4, b 3.6

In the first section of this paper the methodology is presented and validated for both thermal and mechanical models. The validation of the heat transfer numerical model is realized by comparing the experimental measurements with the simulation results, for the heat fluxes at the boundaries of the block. The thermal properties of the concrete material are determined experimentally using a solid concrete sample. The mechanical numerical model based on the “Hognestad stress–strain modified model” is validated by being compared to the experimental measurements of Álvarez-Pérez et al. [21].

In the second section, the thermal and mechanical results for the ten hollow blocks are presented in order to better understand, on the one hand, the effect of the blocks' internal shape on these parameters, and, on the second hand, to compare and promote some block configurations according to their mechanical and thermal performances.

The blocks are traditionally handcrafted and the mixture is made of 25% of fine gravel aggregates (4 - 8 mm) and 75% of powdered stone dust (0.5 - 4 mm). One cubic meter of aggregates is mixed with 50 kg of Portland cement and 50 liters of water to form the solid matrix mixture. The thermal and mechanical properties of the concrete used in this study are summarized in Table 2.

**Table 2- Physical properties of the adopted concrete composing the blocks**

Density ( $\text{kg.m}^{-3}$ )	2300
Heat Capacity at constant pressure ( $\text{J.kg}^{-1}.\text{K}^{-1}$ )	880
Thermal conductivity ( $\text{W.m}^{-1}.\text{K}^{-1}$ )	1.4
Young's modulus (Pa)	$25 \times 10^9$
Compressive strength (Pa)	$30 \times 10^6$
Poisson's ratio (-)	0.2

### 3 Methodology and models validation

#### 3.1 Heat transfer in the hollow blocks

##### 3.1.1 Experimental thermal characterization method

Before performing the numerical heat simulations, the numerical model was validated by comparing the numerical results to the experimental ones for a particular hollow block shape used very frequently in the Lebanese constructions (Model 10).

The tangential gradient flux sensors used in this work use printed circuit technology; they are used in many building thermal applications (Cherif et al. [22] and Zalewski et al. [23]). The schematic construction principle of the sensor is shown in Fig. 1a. These fluxmeters present the advantage of providing a good sensitivity ( $\sim 100 \mu\text{V/W/m}^2$ ).

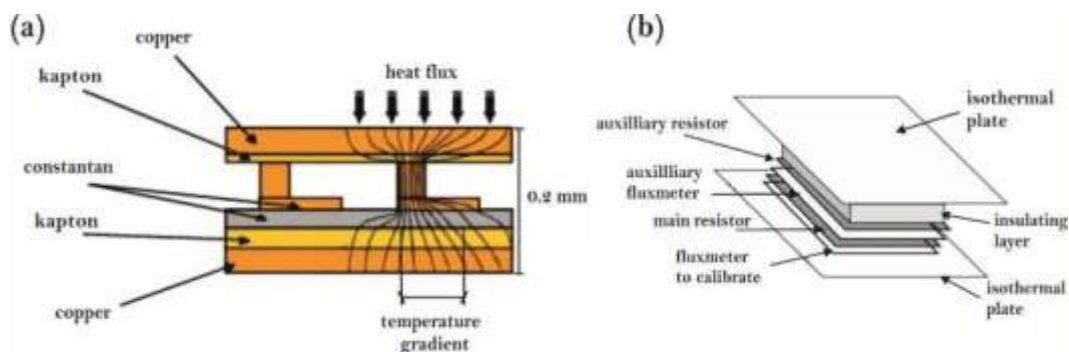


**Figure 1- Schematic drawing of the used heat flux sensors: (a) Heat flux sensor's sketch (b) Calibration apparatus**

The zero-flux method was adopted for the calibration of the fluxmeter for determining its sensitivity and response to thermal solicitations [22, 23]. The fluxmeter to be calibrated is covered with a heating resistor which dissipates a known amount of electrical heat by Joule effect as shown in Fig. 1b. The calibration results provide a relation

between the measured voltage in terms of the injected power. The sensitivity of the sensor defined as the slope of the regression line of the measured points.

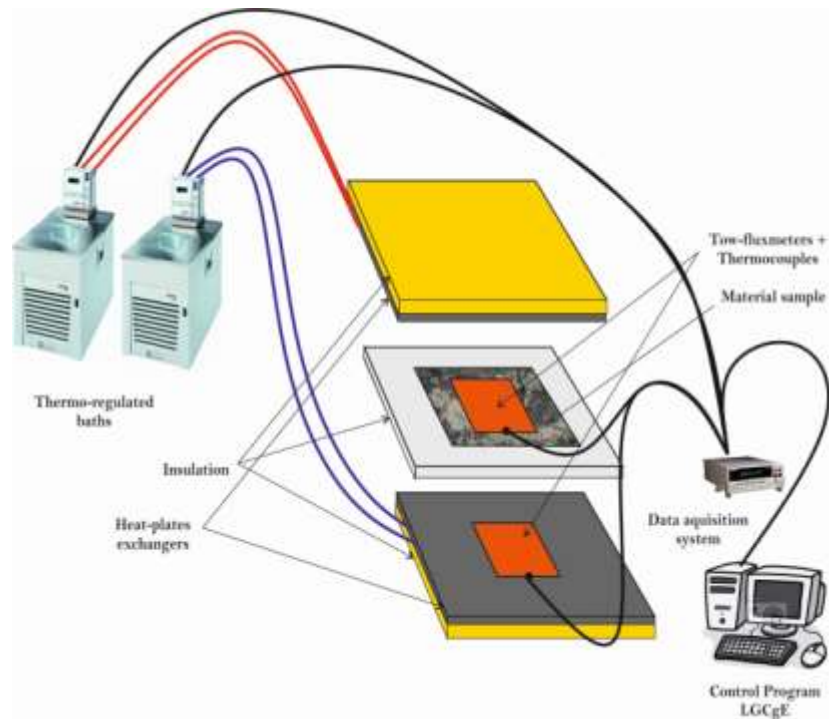


**Figure 2- Experimental device for determination of thermophysical properties of building materials**

The experimental device used for thermal characterization of building materials is described in Fig. 2. It is composed of two thermostatic baths related to two heating plates allowing to impose the temperature boundary conditions on the experimented building material. The heat fluxes and the temperatures on both sides of the sample were simultaneously measured using two thermocouples of *T*-type and two tangential gradient fluxmeters, having an active surface of 0.15 x 0.15 m<sup>2</sup>. The lateral faces of the sample are covered with an insulation material to impose unidirectional heat transfer conditions.

a.) Determination of the thermal conductivity

The method consists in subjecting a sample of thickness "*e*" (m) to a temperature gradient, so as to impose a flux transfer from the hot side to the cold one. The heat flux  $\varphi$  (W.m<sup>-2</sup>) and the temperature on both sides of the sample are measured simultaneously. The Fourier's law applied in unidirectional steady state conditions gives [24]:

$$\varphi_1 = \frac{\Delta T}{R} \text{ and } \varphi_2 = \frac{\Delta T}{R} \quad (1)$$

Eq. 1 can be written in terms of the generalized quantities  $\Sigma\varphi$  (W.m<sup>-2</sup>) and  $\Delta T$  (K) as:

$$\Sigma\varphi = 2 \frac{\Delta T}{R} \quad (2)$$

The thermal resistance  $R$  (m<sup>2</sup>.K.W<sup>-1</sup>) and the thermal conductivity  $\lambda$  (W.m<sup>-1</sup>.K<sup>-1</sup>) are thus given by:

$$R = \frac{2\Delta T}{\Sigma\varphi} \text{ and } \lambda = \frac{e}{R} \quad (3)$$

b.) Determination of the specific heat

Starting from a stable initial steady state, a temperature variation is imposed by changing the set point on one or both sample faces. The average initial temperature of the sample  $\Sigma T_i$  (K) will change, as will the fluxes over each side. After the reestablishment of the steady state, the material has found a new stable state, associated with a new average final temperature  $\Sigma T_f$  (K).

During the transient phase, the relation between the stored (or released) heat energy  $Q$  (J.m<sup>-2</sup>) and the heat fluxes difference  $\Delta\phi$  (W.m<sup>-2</sup>) is given by [24]:

$$Q = \int_{t_i}^{t_f} \Delta\phi . dt \quad (4)$$

It can also be related to average temperatures  $\Sigma T_i/2$  and  $\Sigma T_f/2$ , where  $\Sigma T_i$  and  $\Sigma T_f$  represents the sum of the temperatures on each face at the initial time  $t_i$  (s) and at the final time  $t_f$  (s).

$$Q = C \frac{\Sigma T_f - \Sigma T_i}{2} \quad (5)$$

The heat capacity of the sample  $C$  (J.m<sup>-2</sup>.K<sup>-1</sup>) is thus given by:

$$C = \frac{2 \int_{t_i}^{t_f} \Delta\phi . dt}{\Sigma T_f - \Sigma T_i} \quad (6)$$

The specific heat  $c_p$  (J.kg<sup>-1</sup>.K<sup>-1</sup>) can be deduced knowing the density and the thickness of the sample:

$$c_p = \frac{C}{\rho e} \quad (7)$$

### 3.1.2 Experimental thermal results for the concrete mixture

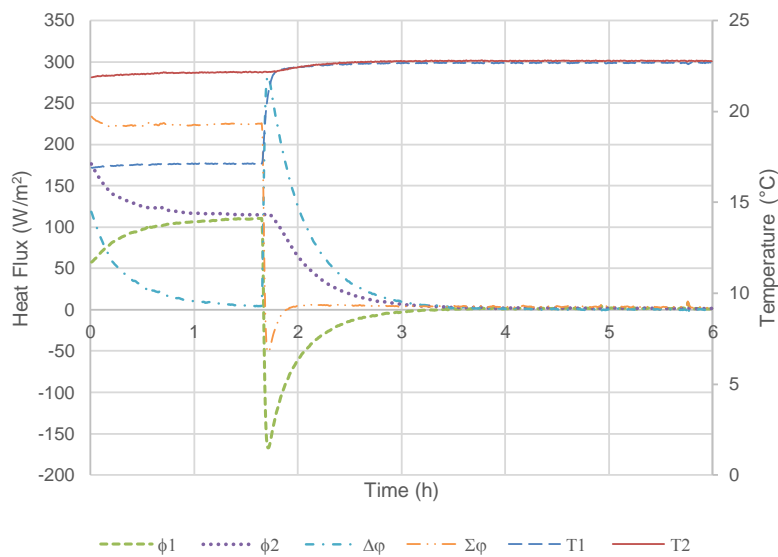


Figure 3- Experimental measurement results for the concrete mixture [24]

Fig. 3 provides the experimental results for the concrete mixture.

Using Eq. (1) and Eq. (3) and based on the experimental results presented in Fig. 3 in steady state conditions ( $\approx 1.6h$ ), the thermal conductivity of the concrete mixture can be determined.

Using Eq. (6) and Eq. (7) and based on the experimental results presented in Fig. 3 in transient conditions ( $1.7h < t < 3.5h$ ), the specific heat of the concrete mixture can be determined.

The determined thermal conductivity and specific heat of the concrete mixture are reported in Table 2.

### 3.1.3 Numerical thermal assessment method

In what follows, and after the validation of the heat transfer model, the different block configurations will be thermally compared based on the following criteria:

- Temperature distribution
- Heat flux distribution
- Dynamic and thermal convection phenomena inside the cavities

A parametric study for different concrete mixture thermal conductivities was also presented to evaluate the effect of the concrete mixture's thermal conductivity on the overall thermal performances of the different block shapes.

The conductive heat transfer mode in the concrete mixture as well as the convective heat transfer inside the cavities, were separately investigated to understand the effect of each heat transfer mode.

The blocks are studied using a 3D geometry in steady state boundary conditions; a temperature gradient of  $20\text{ }^{\circ}\text{C}$  is imposed on the opposite faces of the block ( $0^{\circ}\text{C} - 20^{\circ}\text{C}$ ), the other faces remaining adiabatic as shown in Fig. 4. This gradient was chosen because it is high enough to generate a noticeable heat transfer in the block for a better visualization of heat transfer phenomena and a better precision in the simulated results, while remaining in the temperature range encountered in real life situation in building energy simulation cases.

In the coupled CFD-thermal analysis of the hollow blocks, it is essential to account the three key mechanisms of the heat transfer (i.e., conduction, convection, and radiation). The conduction occurs in the solid concrete mixture while convection and radiation occur inside the block cavities.

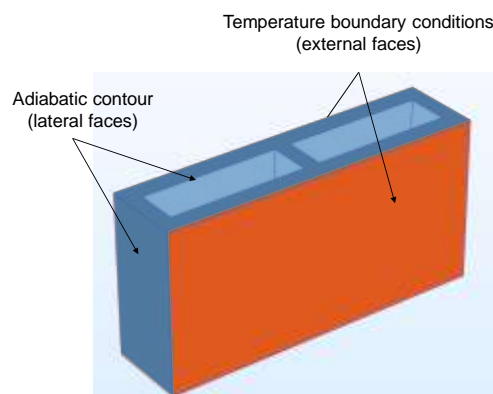


**Figure 4- Imposed temperatures and adiabatic surfaces**

### 3.1.4 Numerical and experimental thermal properties of the Lebanese traditional hollow block

The heat transfer simulation in hollow blocks is based on the thermal properties of the concrete mixture presented in Table 2. The air circulation inside the cavity, promoting the natural convection, was considered as a laminar flow. It is coupled with the radiation model using the discrete ordinates method (DO) and the simulation was performed using the implicit solver of COMSOL Multiphysics®. The air density was assumed to be dependent on pressure and temperature varying according to the ideal gas relation [25]. The validity of the heat transfer model inside the cavities of the blocks has been realized in previous works [24, 26]. The same temperature boundary conditions applied to the block in the experimental test were imposed to the simulated block on the opposite faces, the other faces remaining adiabatic. The typical Lebanese hollow Block (Model 10) was used for the validation of the numerical model.

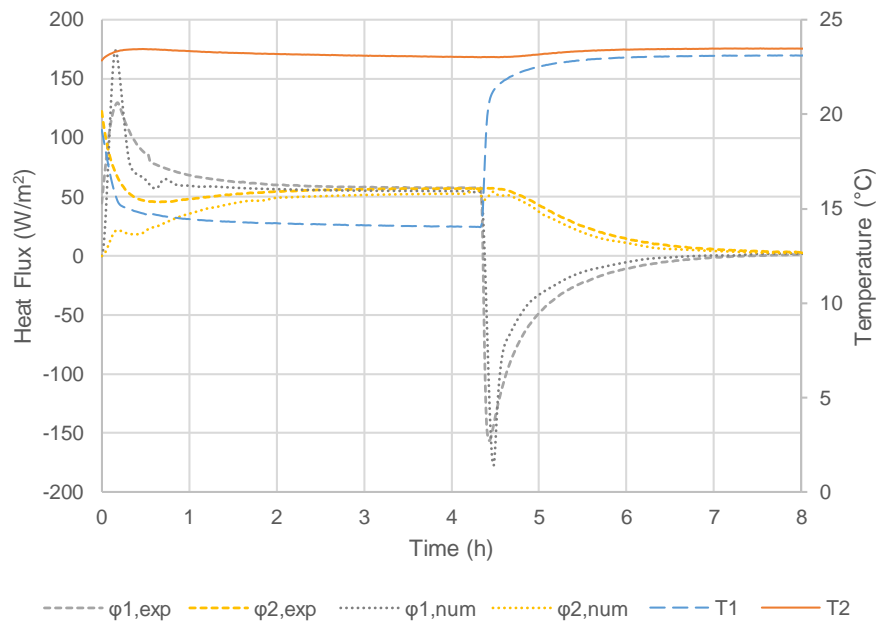


**Figure 5- Experimental measurements and numerical results for the Lebanese traditional concrete hollow block (Model 10) [24]**

Fig. 5, shows the evolution of the imposed temperatures and the measured and simulated heat fluxes on the block faces. The wall is first subjected to a 10°C temperature gradient by imposing about 14°C and 24°C a temperature conditions on its boundary edges. A steady state is reached after about 3 hours. Then, at t~4.2h, the block face subjected to a temperature of 14°C was heated to reach a temperature close to the other face (24°C). The comparison between the numerical results and the experimental measurements for the heat fluxes evolution at the boundaries of the block gives very similar results, except for the first part (between t=0h and t=2h) where the heat flux is affected by the material history (initial conditions) and the heat stored in the material before starting the tests.

In order to define how well the measured and the simulated heat fluxes are identical, the Nash-Sutcliffe Efficiency coefficient (*NSE*) [27] was determined for  $\varphi_1$  and  $\varphi_2$  as shown in Fig. 6. The results indicate a good match between the simulation results and the measurements with *NSE* values close to 1 for both  $\varphi_1$  and  $\varphi_2$ .

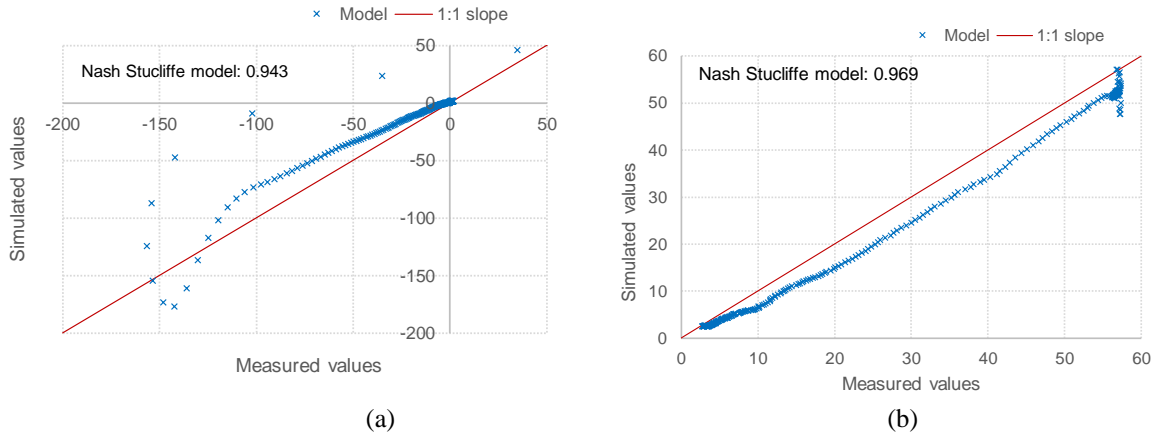


Figure 6- Nash Sutcliffe model for  $\phi_1$  (a) and  $\phi_2$  (b)

### 3.2 Mechanical resistance of the hollow blocks

#### 3.2.1 Validation of the mechanical model

A common representation of the stress–strain curve for concretes with strengths up to about 40 MPa is provided by the “Hognestad stress–strain modified model” [28] shown in Fig. 7. The curve is composed by a second-degree parabola for a strain varying between zero and  $\epsilon_0=1.8f'_c/E_c$  where  $f'_c=0.9f_c$ , then followed by a downward-sloping line terminating at a limiting strain of 0.0038. In the adopted numerical model used for describing the block behavior, the concrete is considered as a nonlinear elastic material following the uniaxial data model provided by the Hognestad modified relation.

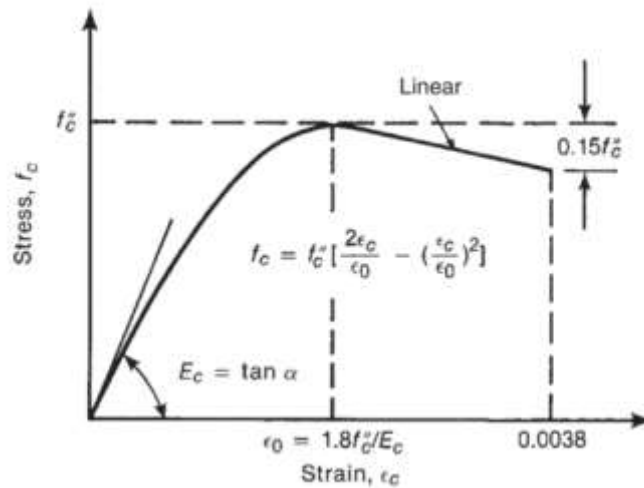
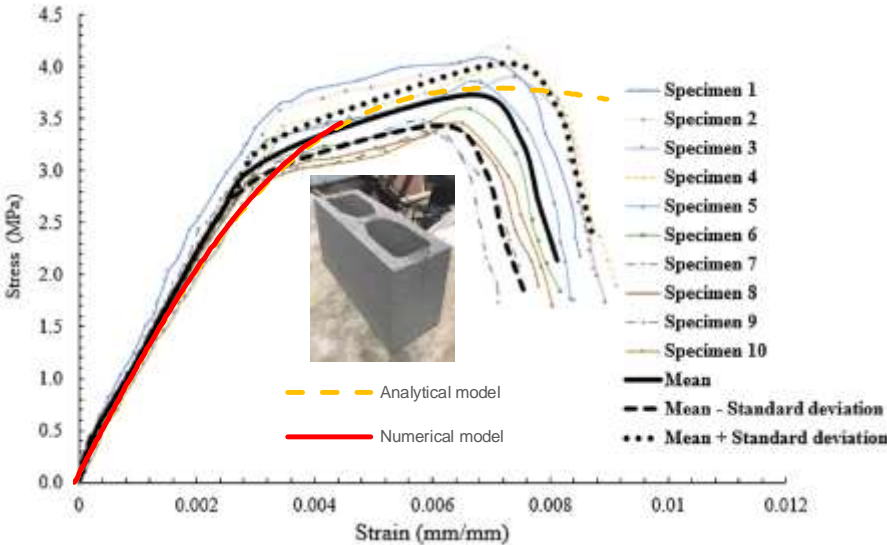


Figure 7- Hognestad modified stress–strain model

The numerical model validation was performed using the experimental results of Álvarez-Pérez et al. [21] who sampled and tested ten hollow blocs according to the standards [29-33]. These double-cell blocks are made with medium sand sieve (59.55%), coarse sand sieve (25.91%), cement CP-40 (10.02%) and water (4.52%), and their dimensions are: 393 mm x 193 mm x 144 mm (length x height x thickness). The hollow block sample was

modelled and simulated using as mechanical properties the mean values of the tested samples (Density 1154 kg.m<sup>-3</sup>, Young Modulus 1056 MPa, Poisson ratio 0.155, and Uniaxial compressive strength 3.74 MPa). One face of the block was subjected to a prescribed displacement load of 1 kN every 10 seconds until reaching the ultimate load capacity (130 kN), the opposite face being subjected to a fixed constraint and the four remaining faces having free boundary conditions. The stress-strain diagram of the ten tested specimen is shown in Fig. 8. The analytical results (Orange curve) and the numerical results (Red curve), which are based on the adopted Hognestad stress–strain modified model, are comparable with the experimental results. The adopted numerical method can thus be validated and that the model can be considered as valid and reliable.



**Figure 8- Comparison between the numerical Hognestad stress–strain modified model and the experimental results obtained by Álvarez-Pérez et al. [21]**

**3.2.2 Numerical mechanical assessment method**

In the numerical assessment, the blocks were subjected to a constant load assumed to be in their elastic loading margin aiming at comparing the stress distribution for each block configuration. At first, a vertical uniform boundary load of 100 kN was applied to the block in the z-axis direction (Fig. 9) and the stresses induced by this load were numerically simulated using the implicit solver of COMSOL Multiphysics® Modeling Software.

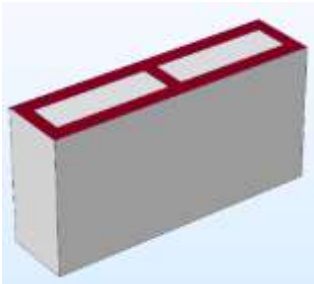


**Figure 9- Boundary load for the compression in the z-axis direction**

The failure criteria used in the study are the ones used for brittle solids and known as the maximum stress/strain criteria. The maximum stress criterion assumes that a material fails if the maximum principal stress  $\sigma_1$  in a material element exceeds its tensile strength  $\sigma_t$ , or alternatively, if the minimum principal stress  $\sigma_3$  is less than its compressive strength  $\sigma_c$ . The safe region for the material is thus:  $\sigma_c < \sigma_3 < \sigma_1 < \sigma_t$ .

Note that the convention that tension is positive has been used in the above expression.

Then, another parameter that is interesting to investigate for the mechanical behavior of the blocks is their compressive strength on their lateral surfaces. In fact, during transportation, storage, and implementation, the blocks experience some harsh conditions in the factory and on site that make their mechanical strength essential for their practical use. Thus, the mechanical resistance of the blocks was also studied according to the  $y$ -axis by applying a uniform boundary load of 10 kN on one face (Fig. 10), the other face being subjected to a fixed constraint.

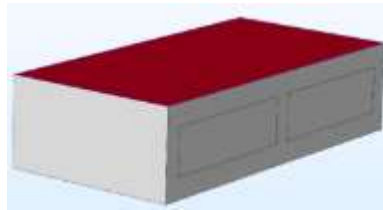


**Figure 10- Boundary load for the compression in the  $y$ -axis direction**

### 3.3 Mesh independence analysis

The mesh independence is verified for Model 1 for both the thermal and mechanical simulation models. Also, the simulation time is evaluated in order to choose the optimal meshing configuration. It is important to mention that the meshing was performed automatically using the “Physics-controlled mesh” module of COMSOL Multiphysics® which allows a better accuracy of the results; this meshing is done depending on the physical property settings, the boundary conditions, and the geometry of the tested model.

Fig. 11 shows the heat flux and the simulation duration for five different mesh configurations (“Extremely coarse”, “Extra coarse”, “Coarser”, “Coarse”, and “Normal”). The heat flux in the  $y$ -direction (perpendicular to the external block faces) stabilizes for an “Extremely coarse” mesh configuration (7436 elements). The simulation time increases from 25s for the “Extremely coarse” meshing (2632 elements) to 2324s (around 40 minutes) for the “Normal meshing” (103109 elements). “Finer” meshing configurations, beyond the “Normal” meshing, were not investigated to avoid very high simulation durations especially that the solution converges for lower meshing. Thereafter, the “Extra coarse” meshing is adopted for its low simulation time (less than two minutes) and its good accuracy.

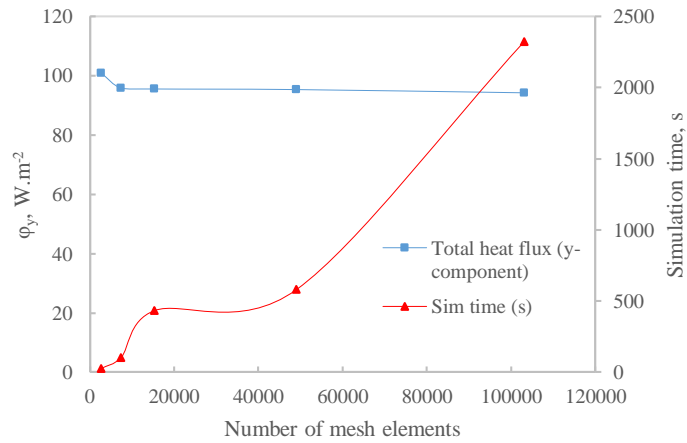


**Figure 11-Variations of the Total Heat Flux in the y-direction, and the total simulation time for different numbers of meshing elements**

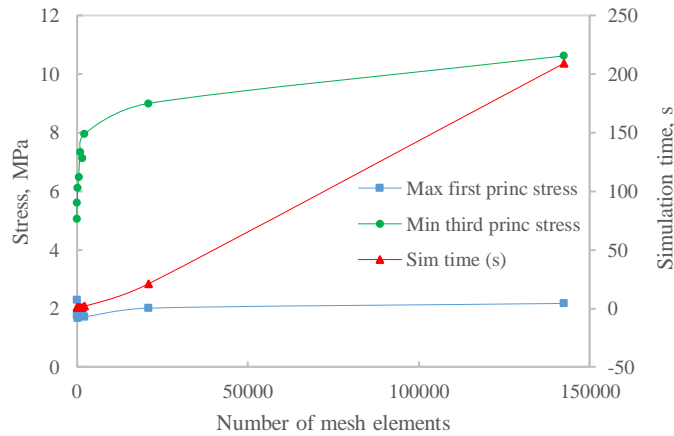


**Figure 12-Variations of Maximum First Principal Stress, the Minimum Third Principal Stress, and the total simulation time for different numbers of meshing elements**

Fig. 12 represents the Maximum First Principal Stress and the Minimum Third Principal Stress as well as the simulation duration for nine different mesh configurations (“Extremely coarse”, “Extra coarse”, “Coarser”, “Coarse”, “Normal”, “Fine”, “Finer”, “Extra fine”, and “Extremely fine”). The Maximum First Principal Stress and Minimum Third Principal Stress require an “Extremely fine” meshing (142473 elements) to stabilize. The simulation time is relatively low compared to the heat transfer model and does not exceed four minutes for the “Extremely fine” meshing. In what follows, the “Extremely fine” meshing is adopted.

4 Results and discussion

4.1 Heat transfer analysis

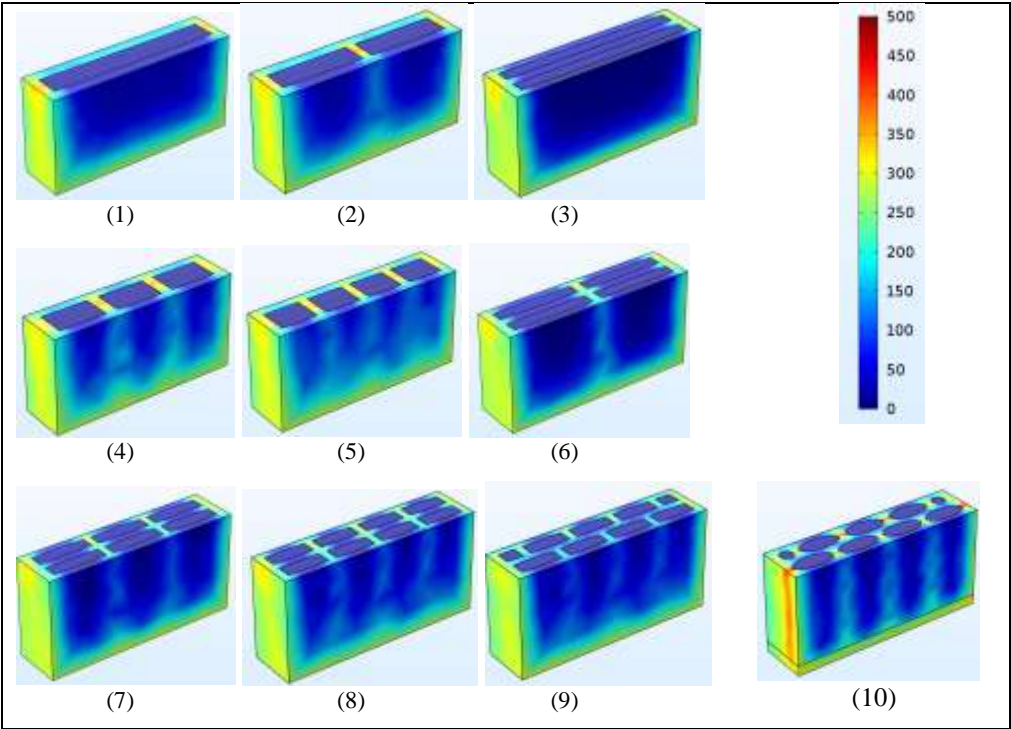


Figure 13- Total heat flux in the y-direction ( $W.m^{-2}$ )

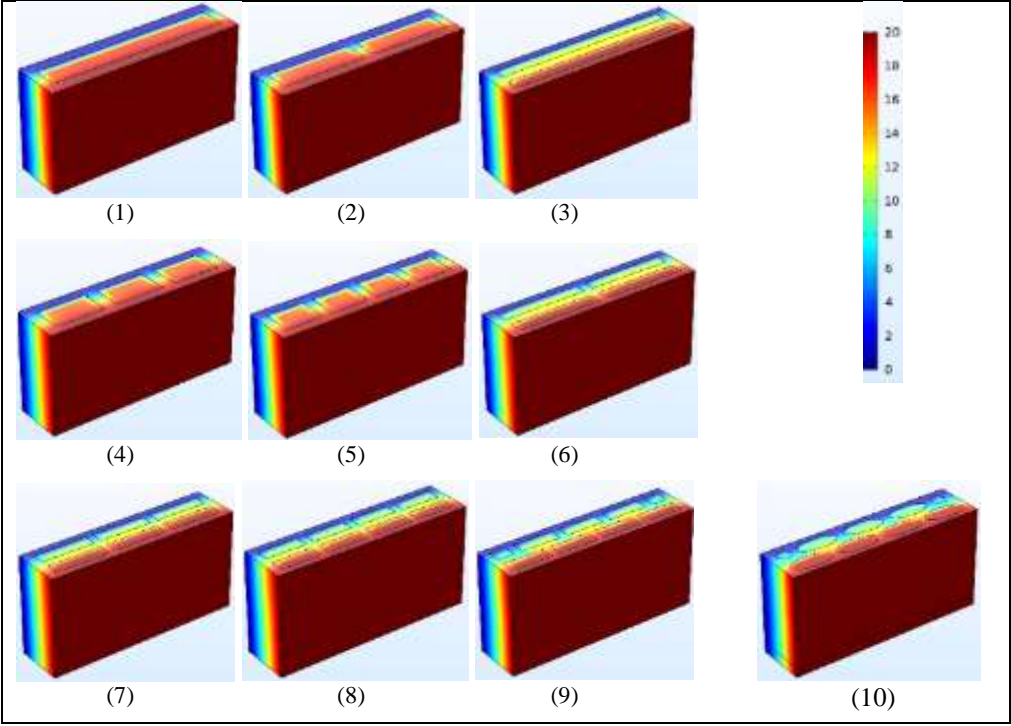


Figure 14- Temperature distribution in the blocks ( $^{\circ}C$ )

A thermal conductivity of  $1.4 W.m^{-1}.K^{-1}$  was considered for the concrete mixture.

Fig. 13 clearly shows the effect of longitudinal and transversal bulkheads on the conductive heat transfer in the different hollow block configurations. The longitudinal bulkheads improve the thermal resistance of the blocks and thus reduce the heat flux passing through the blocks. This can be clearly observed by comparing Models 1 and 3, Models 2 and 6, Models 4 and 7, and Models 5 and 8 respectively. Indeed, the external face of the blocks presenting a central longitudinal bulkhead (3, 6, 7, and 8) is darker than the face of the ones without a central longitudinal bulkhead (1, 2, 4, and 5) which means that the heat flux in the block with longitudinal bulkheads is lower than that in the blocks with transversal bulkheads. On the other hand, the transversal bulkheads reduce the thermal performance of the hollow blocks by creating heat bridges inside their structure, this can be observed by comparing Models 1, 2, 4, and 5.

Fig. 14 shows the temperature fields in the different studied blocks shapes and for a temperature difference of 20°C. Unlike the heat flux distribution that is highly dependent from the cavities number and shapes, the temperature distribution is very similar for the studied blocks. When the blocks possess one longitudinal row of cavities, the color of the cavities is mostly orange with one yellow colder side and one red warmer side, this is the case of the block models 1, 2, 4, and 5. However, when the blocks possess two longitudinal rows of cavities, the first row is mostly yellow with one blue colder side and one yellow warmer side, while the second row is mostly red with one yellow colder side and one red warmer side. Two facts can be confirmed from these observations:

- 1.) the temperature drop takes place mostly in the cavities which means that the cavities present the main barrier for the heat transfer in the hollow blocks.
- 2.) the addition of a row of cavities creates more separation in the temperature distribution inside the blocks keeping one part warm and the other part cold creating more separation in the temperature distribution inside the blocks keeping one part warm and other part cold. This will improve the thermal comfort inside the building and reduce thermal losses across the walls' surfaces.

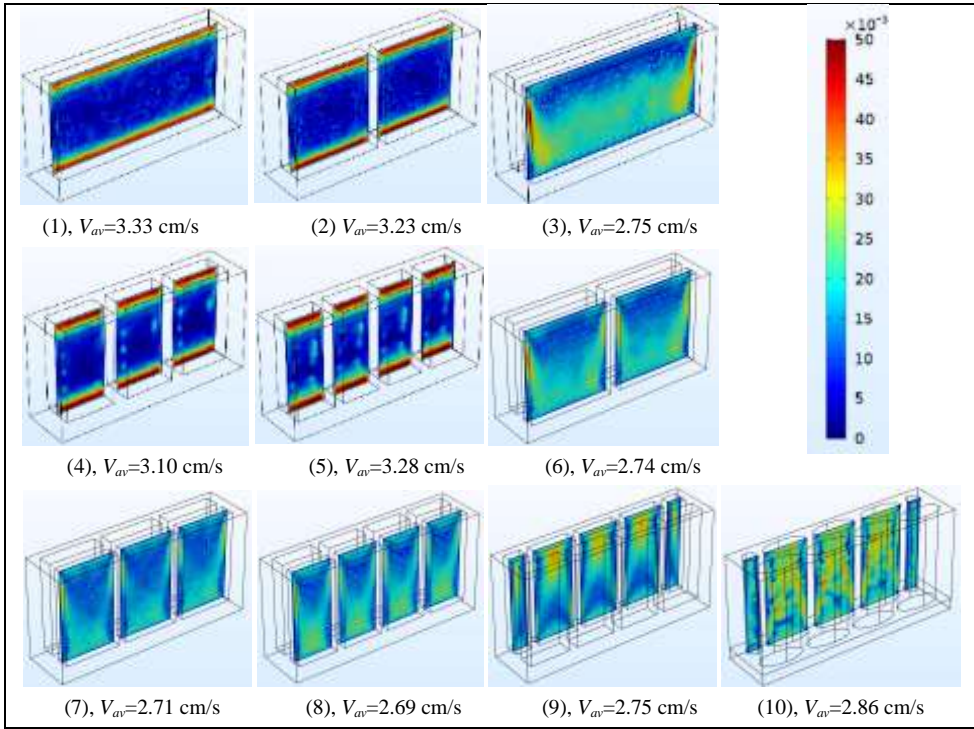


Figure 15- Air velocity magnitude inside the cavities (m/s)

Furthermore, the average air velocity magnitude inside the cavities, reflecting the occurrence of natural convection, depends mainly on the number of longitudinal cavities. The hollow blocks presenting one row of cavities (Models 1, 2, 4, and 5) have higher velocity magnitudes as shown in Fig. 15 with average velocities exceeding 3 cm/s; while the remaining Models, presenting 2 rows of cavities, have lower average velocities less than 3 cm/s. On the other hand, adding adjacent cavities reduces slightly the air velocity in the cavities; this can be observed by comparing the average velocities in Models 1, 2, 4, and 5. The lower air velocities are inside the cavities, the lower are convective heat transfer currents, and the more insulating are the hollow blocks. Moreover, the comparison between models 9 and 10 shows that the elliptical cavity shape increases the air acceleration at the edges of the cavity leading to an increase in convective heat transfer inside the hollow block.

Fig.16 shows the streamlines (left) and the isotherms (middle) for a vertical section in each block (right). For the streamlines, one can notice that the blocks presenting a single longitudinal series of the cavities, the curves form very dispersed and clearly visible elliptical recirculation zones occupying the entire volume of the cavities, these curves record maximum speeds of around 7cm/s at the edges of the cavities, which promotes and accelerates the convective heat transfer inside the blocks. One can also notice that the air velocity decreases while moving away from the edges of the cavities and the center of the cells remains almost inert. The remaining models presenting two longitudinal series of the cavities, the average maximum speed is around 5cm/s or less; the effect of convection is less favored in these models, the streamlines are very tight and take the form of a baguette shape.

The analysis of the isotherms allowing the distribution of the curves is divided into two families of shape.

- 1.) The first family includes the models presenting one longitudinal row of cavities (1, 2, 4 and 5) where the isotherms present a sinusoidal shape tendency. The temperature shape results from the movement of convection recirculation in the air cavities with an upward movement near the hot wall and a downward movement on the cold wall side. A relatively high thermal gradient is observed between the two opposing cavity walls reaching 14.5°C. The isotherms present blue tendency in the bottom of the cavities and red tendency at the top, which is due to thermal stratification where cooler and denser air sinks, and warmer and thinner air rises creating layers of air with a gradient of temperatures.
- 2.) On the other hand, the second family of curves which groups models (3, 6, 7, 8, 9 and 10), the shape of the curves gives a moderately linear tendency remaining very tight and confined in the spaces where the boundary layers are very close to the cavity walls. As these models present two longitudinal series of the cavities, we observe the formation of two cells presenting symmetrical isotherms shapes (since the blocks are symmetrically heated) and different colors, red and yellow colors are observed inside the cavities near the hot block side, and green and blue colors are observed inside the cavities near the cold block side. The thermal gradient in each cell (hot or cold) is around 8.5 ° C.

In summary, the convective transfer is widely present in concrete hollow blocks whatever their shape is. From a dynamic and thermal perspective, one can found that the nature of the thermal transfer differs from one block to another at both quantitative and qualitative levels.

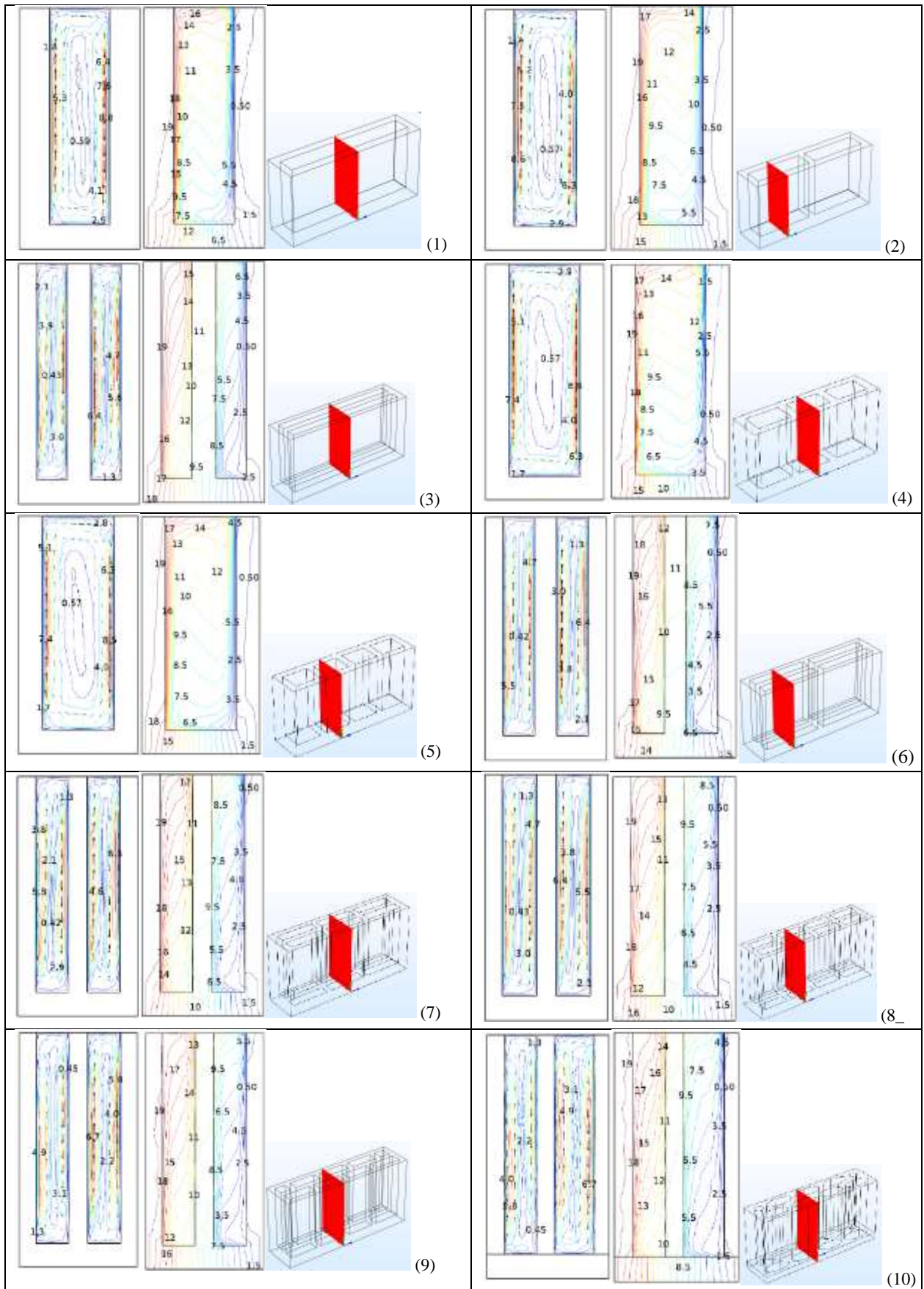
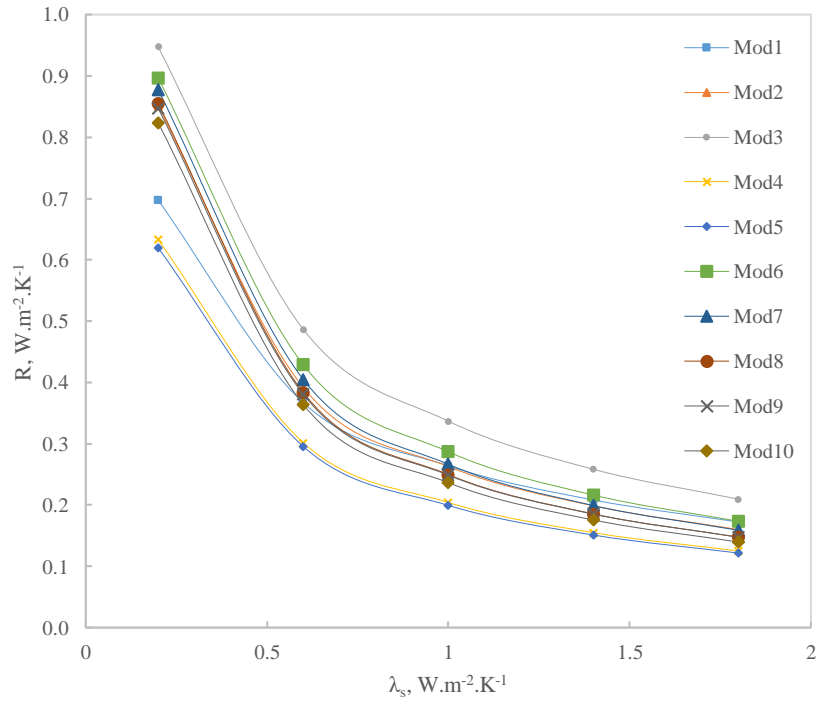


Figure 16- Air velocity field contour (cm.s<sup>-1</sup>) and isotherms (°C) inside vertical cross planes for the ten investigated models

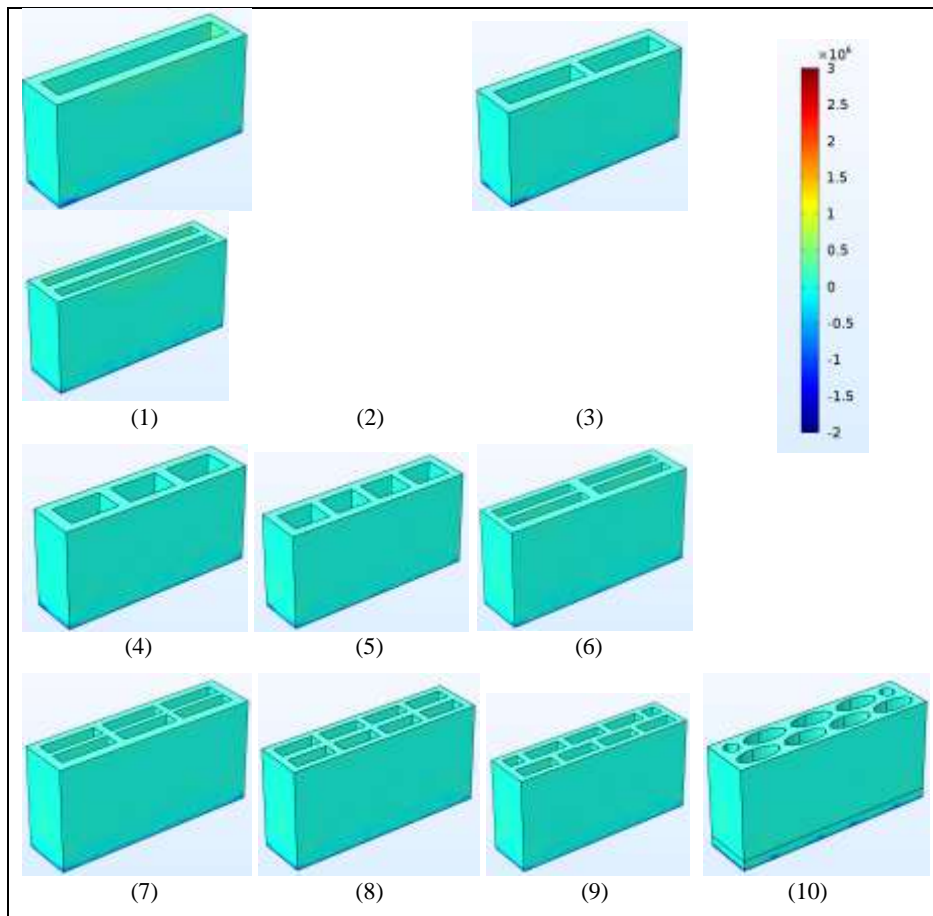


**Figure 17- Equivalent thermal resistance versus concrete mixture thermal conductivity for different configurations**

Furthermore, the thermal conductivity of the concrete mixture was varied between  $0.2 \text{ W.m}^{-1}.\text{K}^{-1}$  and  $1.8 \text{ W.m}^{-1}.\text{K}^{-1}$  in order to study the effect of the concrete mixture on the overall thermal performances of the different block shapes.

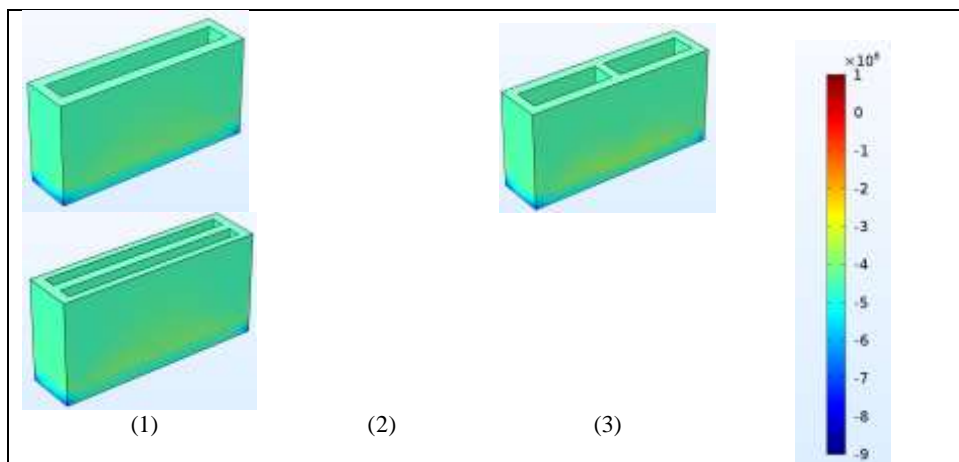
The parametric study for different concrete mixture thermal conductivities represented in Fig. 17 for the ten investigated models, shows that the best thermal configuration is obtained by Model 3 (two parallel cavities) and the worst case is for Model 5 (four adjacent cavities). A thermal resistance difference of 40% to 60% is noticed between these two models depending on the thermal conductivity of the concrete. The results of Fig. 17 confirm the observations of Fig. 13 showing the effect of longitudinal and transversal bulkheads (by maintaining a same void ratio).

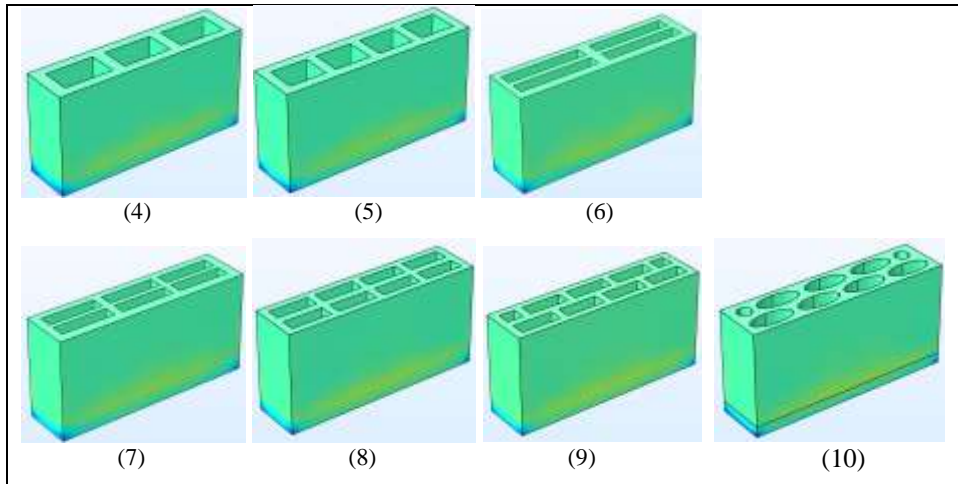
## 4.2 Mechanical behavior, compression z-axis



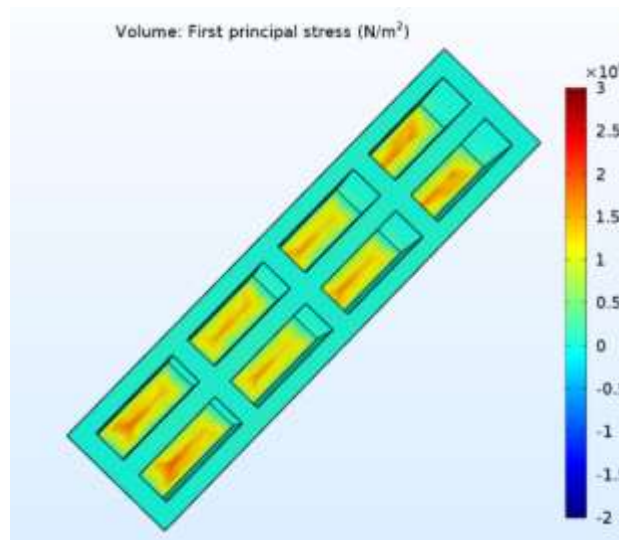
**Figure 18- First principal stress distribution for z-axis compression (MPa)**

Fig. 18 and Fig. 19 show a very similar stress distribution for the first and third principal stresses in the ten different investigated hollow blocks. The visualization of the results shows no favor for a particular block configuration when it comes to mechanical resistance to vertical compression in the z-direction; this is mainly due to the fact that the blocks were chosen so as to have similar void ratios and therefore similar active area against compression.





**Figure 19- Third principal stress distribution for  $z$ -axis compression (MPa)**



**Figure 20- Stress concentration inside the block cavities (MPa)**

The critical zone for the third principal stress (compressive stress) is at the bottom of the blocks and more specifically at the corners (Fig. 19). The critical zone for the first principal stress (tensile stress) is at the bottom of the blocks inside the cavities as shown in Fig. 20.

#### **4.3 Mechanical behavior, compression $y$ -axis**

The side compression of the blocks ( $y$ -axis) has an important impact on the adequate selection of the blocks since the blocks are designed to support various loads and often undergo various loads during their transport, storage, and implementation.

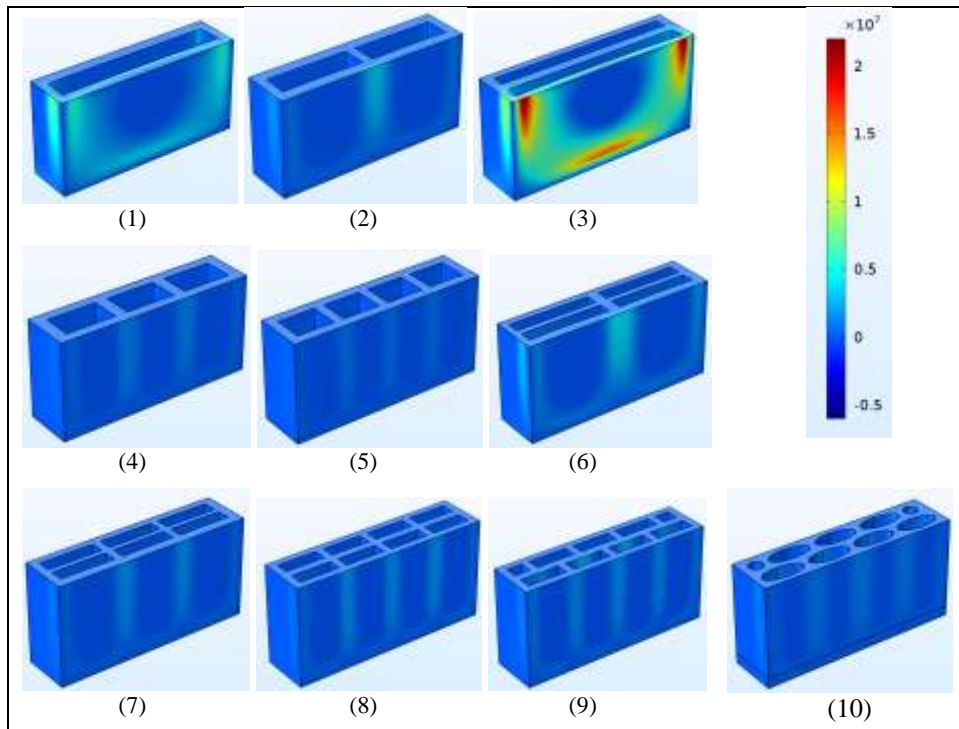


Figure 21- First principal stress distribution for y-axis compression (MPa)

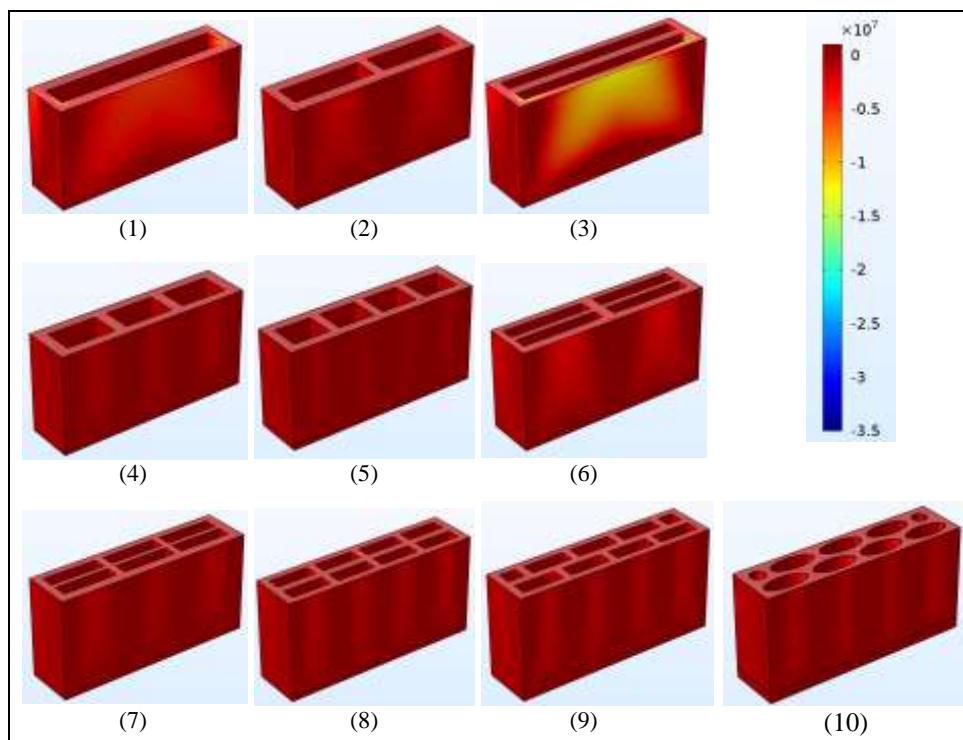


Figure 22- Third principal stress distribution for y-axis compression (MPa)

The results in Fig. 21 and Fig. 22 clearly show the vulnerability of Model 3, and less markedly Model 1, compared to the other models. The very low thickness of the longitudinal bulkheads (1.5 cm) and the absence of transversal bulkheads cause a weak resistance to side compression (y-axis) and thus a high stress concentration at the edges of

the lateral area of the block. The resistance to side compression increases by increasing the transversal bulkheads and decreasing the longitudinal bulkheads.

The mechanical behavior of the investigated blocks varies very slightly in compression in the z-axis which reduces the influence of this parameter in the selection of the best shape configuration. This is mainly due to the initial assumption of selecting blocks having approximatively similar void ratios of about 40%, and thus implies comparing blocks with same active area in compression test.

#### 4.4 Final results & discussion

The mechanical and thermal results are summarized in Table 4. Knowing that the compressive strength for concrete varies from less than 10 N/mm<sup>2</sup> for lean concretes to more than 55 N/mm<sup>2</sup> for special concretes, and the tensile strength of concrete is usually considered about one-tenth of its compressive strength [34], it can be clearly concluded from Table 3 that the first principal stress is the main criterion of failure that needs to be verified when studying hollow block concrete samples. Indeed, the maximum first principal stress is found to be always higher than one-tenth of the minimum third principal stress (in absolute value).

**Table 3- Summary of the mechanical and thermal results**

				z-compression (100kN)			y-compression (10kN)		
Models	Model #	$R_{eq}$ (m <sup>2</sup> .K/W)	U-value (W/m <sup>2</sup> .K)	$\sigma_{1max}$ (MPa)	$\sigma_{3min}$ (Mpa)	$\sigma_{av}$ (Mpa)	$\sigma_{1max}$ (MPa)	$\sigma_{3min}$ (Mpa)	$\sigma_{av}$ (Mpa)
1 cavity	1	0.209	5.613	1.81	-7.34	-4.22	7.43	-16.89	-0.85
2 cavities by side	2	0.199	6.220	1.75	-7.19	-4.23	3.24	-4.89	-0.38
2 cavities parallel	3	0.258	4.255	1.77	-6.86	-4.23	21.56	-34.13	-1.07
3 cavities by side	4	0.154	6.931	1.7	-7.12	-4.22	1.31	-2.46	-0.28
4 cavities by side	5	0.151	7.441	1.73	-7.22	-4.22	0.83	-1.42	-0.25
4 cavities 2 x 2	6	0.217	4.787	1.73	-6.73	-4.18	3.99	-6.54	-0.41
6 cavities 3 x 2	7	0.199	5.488	1.78	-6.71	-4.2	1.79	-3.15	-2.96
8 cavities 4 x 2	8	0.185	5.820	1.94	-6.56	-4.22	1.71	-2.79	-0.28
8 cavities + alternation	9	0.186	5.787	1.93	-6.72	-4.14	2.43	-3.43	-0.35
Lebanese hollow block	10	0.175	5.942	2.75	-8.51	-4.2	1.31	-3.37	-0.34

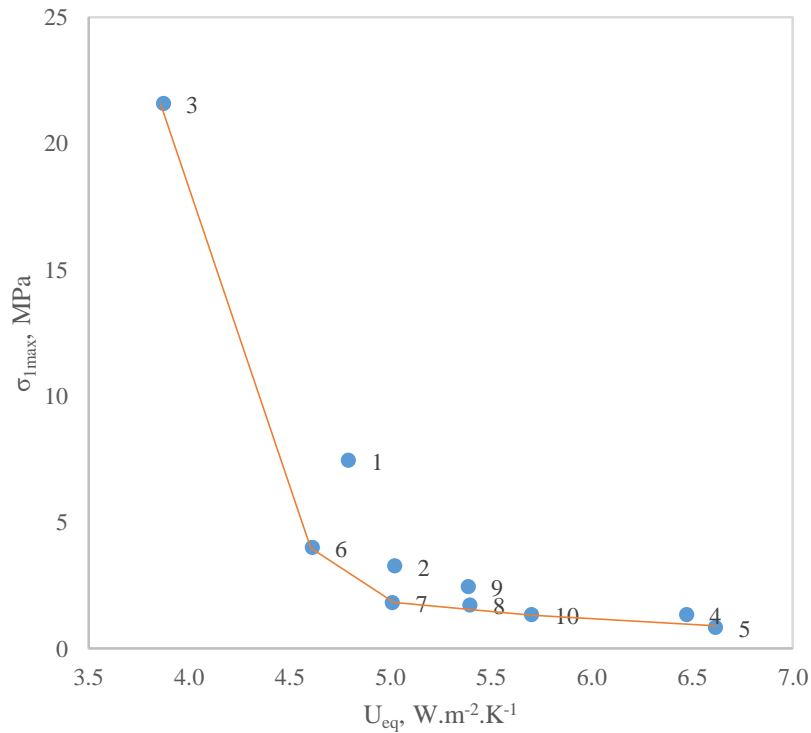


**Figure 23- Pareto chart of the first principal stress distribution for y-axis compression and the  $U$ -value for the ten investigated block configurations**

Fig. 23 shows that the more the  $U$ -value is low (high thermal resistance), the higher is the first principal strength related to side compression, and the less mechanically resistant is the block. The lateral strength of the block and its thermal resistance are thus inversely proportional. The optimal models are Model 3, Model 5, Model 6, Model 7, and Model 10. Model 3 is the most thermally resistant (lowest  $U$ -value) while model 5 has the best lateral strength. Models 6, 7, and 10 present an optimum compromise between thermal and mechanical performances. Models 1, 2, 8, 9, and 4 are less interesting, since there exists a better block configuration on both thermal and mechanical levels.

## 5 Conclusion

A numerical analysis was performed for understanding the main heat transfer phenomena and the mechanical behavior of the concrete hollow block. A parametric study is performed to understand the effect of the geometry configuration on the overall thermal and mechanical resistances of the block. The ten investigated blocks present different inner shape configurations and preserve the same external dimensions (40cm x 20cm x 10cm) for ergonomic reasons as well as local workmanship techniques. The simulation results indicated that the longitudinal bulkheads improve the thermal resistance of the blocks and thus, reduce the heat flux passing through the blocks, while the transversal bulkheads reduce the thermal performance of the hollow blocks by creating heat bridges inside their structure. On the other hand, the mechanical behavior of the investigated blocks varies very slightly between the investigated models in vertical compression in the  $z$ -axis direction which reduces the influence of this

parameter in the selection of the best shape configuration. However, the mechanical resistance to side compression increases by increasing the transversal bulkheads and decreasing the number of longitudinal bulkheads.

Five optimal models can be considered for having interesting mechanical and/or thermal performances (Model 3, 5, 6, 7 and 10). Model 3 possesses the best configuration from a thermal point of view (lowest  $U$ -value), while model 5 is the most performant in lateral mechanical resistance. Models 6, 7, and 10 present an optimum compromise between thermal and mechanical performances. The existing Lebanese hollow block shape (Model 10) presents therefore a good compromise between thermal performance and mechanical strength. This configuration also offers many other practical advantages such as:

- Ease of craftwork demolding
- Ease of implementation by being easy to break to obtain fraction of blocks (half block or quarter block)
- Ease of creating passages for the pipes and electric cables in masonry walls without crumbling the blocks

The conclusions drawn from this work provide valuable data for improving concrete hollow blocks design by highlighting the main parameters that influence the mechanical and thermal performance of concrete masonry hollow blocks.

### **Acknowledgement**

This work is supported by a Grant from the Lebanese University and the LGCgE Laboratory.

### **Compliance with Ethical Standards**

The authors declare that they have no conflict of interest.

### **References**

- [1] Meng Y., Ling T., Mo K. (2018). *Recycling of wastes for value-added applications in concrete blocks: An overview*, Resources, Conservation & Recycling, vol. 138, 298-312.  
DOI: 10.1016/j.resconrec.2018.07.029
- [2] Fraile-Garcia E., Ferreiro-Cabello J., Mendivil-Giro M., San Vicente-Navarro A. (2018). *Thermal behavior of hollow blocks and bricks made of concrete doped with waste tyre rubber*, Construction and Building Materials, vol. 176, 193–200.  
DOI: 10.1016/j.conbuildmat.2018.05.015

- [3] Zhu L., Dai J., Bai G., Zhang F. (2015). *Study on thermal properties of recycled aggregate concrete and recycled concrete blocks*, Construction and Building Materials, vol. 94, 620–628.  
DOI: 10.1016/j.conbuildmat.2015.07.058  
DOI: 10.1016/j.jobe.2018.04.029
- [4] Urban B., Engelmann P., Kossecka E., Kosny J. (2011). *Arranging Insulation for Better Thermal Resistance in Concrete and Masonry Wall Systems*, 9th Nordic Symposium on Building Physics, Finland.  
DOI: 10.1016/j.applthermaleng.2017.04.163
- [5] Fogiatto M. A., Santos G. H., Mendes N. (2016). *Thermal transmittance evaluation of concrete hollow blocks*, 12th Int. Conference on Heat Transfer, Fluid Mechanics and Thermodynamics, Spain.
- [6] Kanellopoulos G., Koutsomarkos V. G., Kontoleon K. J., Georgiadis-Filikas K. (2017). *Numerical Analysis and Modelling of Heat Transfer Processes through Perforated Clay Brick Masonry Walls*, Int. Conference on Sustainable Synergies from Buildings to the Urban Scale, Greece.
- [7] Coz Diaz J. J., Garcia Nieto P. J., Dominguez Hernandez J., Suarez Sanchez A. (2009). *Thermal design optimization of lightweight concrete blocks for internal one-way spanning slabs floors by FEM*, Energy and Buildings, vol. 41, 1276–1287.
- [8] Zhang Y., Dua K., Hec J., Yanga L., Li Y., Li S. (2014). *Impact factors analysis on the thermal performance of hollow block wall*, Energy and Buildings, vol. 75, 330–341.  
DOI: 10.1016/j.enbuild.2014.02.037
- [9] Martínez M., Huygen N., Sanders J., Atamturktur S. (2018). *Thermo-fluid dynamic analysis of concrete masonry units via experimental testing and numerical modeling*, J. Building Engineering, vol. 19, 80–90
- [10] Barbosa C. S., Hanai J. B., Lourenco P. B. (2010). *Numerical validation of compressive strength prediction for hollow concrete blocks*, 8th Int. Masonry Conference 2010 in Dresden, Germany
- [11] Ben Ayed H., Limam O., Aidi M., Jelidi A. (2016). *Experimental and numerical study of Interlocking Stabilized Earth Blocks mechanical behavior*, J. Building Engineering, vol. 7, 207-216  
DOI: 10.1016/j.jobe.2016.06.012
- [12] Arun A., Hemalatha G. (2020). *Characteristics of expanded polystyrene (EPS) and its impact on mechanical and thermal performance of insulated concrete form (ICF) system*, Structures, vol. 23, 204–213.  
DOI: 10.1016/j.istruc.2019.10.019
- [13] Javadi A., Badiie H., Sabermahani M. (2018). *Mechanical properties and durability of bio-blocks with recycled concrete aggregates*, Construction and Building Materials, vol. 165, 859–865.  
DOI: 10.1016/j.conbuildmat.2018.01.079
- [14] Coz Díaz J. J., García Nieto P. J., Álvarez Rabanal F. P., Martínez-Luengas A. (2011). *Design and shape optimization of a new type of hollow concrete masonry block using the finite element method*, Engineering Structures, vol. 33, 1–9  
DOI: 10.1016/j.engstruct.2010.09.012
- [15] Javidan F., Safarnejad M., Shahbeyk S. (2013). *Shape Optimization of Hollow Concrete Blocks Using the Lattice Discrete Particle Model*, Iranica J. Energy & Environment. vol. 4, 243-250.  
DOI: 10.5829/idosi.ijee.2013.04.03.10

- [16] Caruana C., Grima C., Yousif C., Buhagiar S., Curmi R. (2017). *Determination of thermal characteristics of standard and improved hollow concrete blocks using different measurement techniques*, J. Building Engineering, vol. 13, 336–346.  
DOI: 10.1016/j.jobe.2017.09.005
- [17] Mohammed B., Hossain A., Swee J., Wong G., Abdullahi M. (2011). *Properties of crumb rubber hollow concrete block*, J. Cleaner Production, vol. 23, 57-67.  
DOI: 10.1016/j.jclepro.2011.10.035
- [18] Su H., Wu D., Shen M., Chen W., Wang S. (2019). *Development and Performance Test including Mechanical and Thermal of New Tenon Composite Block Masonry Walls*, Advances in Materials Science and Engineering, vol. 2019, 1-11.  
DOI: 10.1155/2019/5253946
- [19] Sutcu M., Coz Díaz J. J., Álvarez Rabanal F. P., Gencel O., Akkurt S. (2014). *Thermal performance optimization of hollow clay bricks made up of paper waste*, Energy and Buildings, vol. 75, 96–108.  
DOI: 10.1016/j.enbuild.2014.02.006
- [20] Xu R., He T., Da Y., Liu Y., Li J., Chen C. (2019). *Utilizing wood fiber produced with wood waste to reinforce autoclaved aerated concrete*, Construction and Building Materials, vol. 208, 242–249.  
DOI: 10.1016/j.conbuildmat.2019.03.030
- [21] J. Álvarez-Pérez, J. Chávez-Gómez, B. Terán-Torres, M. Mesa-Lavista, R. Balandrano-Vázquez, *Multifactorial behavior of the elastic modulus and compressive strength in masonry prisms of hollow concrete blocks*, Construction and Building Materials, vol. 241, no. 118002, 2020  
DOI: 10.1016/j.conbuildmat.2020.118002
- [22] Cherif Y., Joulín A., Zalewski L., Lassue S. 2009. *Superficial heat transfer by forced convection and radiation in a horizontal channel*, Int. J. Thermal Sciences, vol. 48, 1696–1706.
- [23] Zalewski L., Lassue S., Roussel D., Boukhalfa K., 2010. *Experimental and numerical characterization of thermal bridges in prefabricated building walls*, Energy Conversion and Management, vol. 51, 2869–2877.
- [24] Sassine, E., Cherif, Y., Dgheim, J. et al. “*Experimental and Numerical Thermal Assessment of Lebanese Traditional Hollow Blocks*”. Int J Thermophys 41, 47 (2020).  
DOI: 10.1007/s10765-020-02626-7
- [25] De Vahl Davis G. (1983). *Natural convection of air in a square cavity, a benchmark numerical solution*, Int. J. Numerical Methods Fluids 3, 249–264.  
<https://doi.org/10.1002/flid.1650030305>
- [26] Sassine E., Cherif Y., Dgheim J., Antczak E. (2020). *Experimental and numerical thermal assessment of EPS concrete hollow blocks in Lebanon*, J. Materials in Civil Engineering, Vol. 32, no. 8, August 2020.  
DOI: 10.1007/s10765-020-02626-7
- [27] AgriMetSoft (2019). Online Calculators. Available on:  
<https://agrimetsoft.com/calculators/Nash%20Sutcliffe%20model%20Efficiency%20coefficient>
- [28] MacGregor J. G. (1992). *Reinforced concrete mechanics and design*, Prentice-Hall, Inc, Englewood Cliffs, NJ.
- [29] ONNCCE, Nacional Organization for Standards and Certification of Construction and Building 2016-2019. <https://onncce.org.mx/es/>

- [30] NMX-C-036-ONNCCE-2013, Compressive strength blocks, partitions or bricks and partitions and paving stones (in Spanish), 2013, p. 10.
- [31] ASTM-C-140, Standard test methods for sampling and testing concrete masonry units and related units, 2018, p. 17.
- [32] ASTM-C-90, Standard specification for loadbearing concrete masonry units, 2016, p. 5.
- [33] ASTM-C-129, Standard specification for nonloadbearing concrete masonry units, 2017, p. 3.
- [34] Surahyo A. (2002). *Concrete Construction, Practical Problems and Solutions*, Oxford University Press.  
DOI: 10.1007/978-3-030-10510-5